International Journal of Thermophysics, Vol. 26, No. 4, July 2005 (© 2005)
DOI: 10.1007/s10765-005-6711-y

Advances in the Experimental Determination of the Uranium–Oxygen Phase Diagram at High Temperature[1]

D. Manara,[2] R. Pflieger,[2] and M. Sheindlin[2,3]

Due to its complex phase diagram and the employment of UO_2 as a nuclear fuel, the binary system U–O is of great interest both scientific and technological. Numerous experimental and theoretical studies have been carried out in the last 45 years in order to determine the properties of this system, leading to a precise definition of a considerable part of the state diagram in the region ranging from pure uranium to stoichiometric UO_2, and at temperatures lower than 1500 K, up to the oxide U_4O_9. However, due to the poor chemical stability of O–U compounds with high oxygen content at high temperature (O/U > 2, $T > 2000$ K), an important part of the phase diagram still lacks experimental data. In this work measurements are presented on the melting transition of the stoichiometric and hyperstoichiometric dioxide UO_{2+x} up to $x = 0.21$, and on the melting point of the higher oxide U_3O_8. These measurements were performed under buffer gas pressures varying between 10 and 250 MPa, using a method based on subsecond laser heating developed to overcome experimental difficulties encountered by previous researchers.

KEY WORDS: containerless techniques; high temperature; laser heating; nuclear fuel; phase diagrams; self-crucible heating; uranium; uranium oxides.

1. INTRODUCTION

Besides the technological importance of UO_2 as nuclear fuel, the system U–O is of great scientific interest, due to the complex behavior of uranium under oxidation. Uranium dioxide crystallizes in the cubic fluorite

[1] Paper presented at the Seventh International Workshop on Subsecond Thermophysics October 6–8, 2004, Orléans, France.

[2] European Commission, JRC, Institute for Transuranium Elements, P.O. Box 2340, 76125 Karlsruhe, Germany.

[3] To whom correspondence should be addressed. E-mail: michael.sheindlin@itu.fzk.de

structure. Non-stoichiometry constitutes a particular feature of this compound, allowed by the presence of a partially filled 5f shell in uranium and the possibility for a U atom to shift easily among the valences from +3 to +6. The species UO_{2+x} can exist, at sufficiently high temperature, as a solid solution over approximately the range $-0.4 < x < +0.3$. At higher oxidation levels, the most stable compound is U_3O_8, which is obtained by heating any lower oxide of uranium in air at temperatures higher than approximately 1000 K [1].

The determination of the phase-transition boundaries for the system U–O is of great importance in the nuclear industry. Knowledge about the melting transition in the nuclear fuel is particularly important in the analysis of hypothetical meltdown accidents, as it defines the structural limit of a combustible element. Moreover, due to a possible failure of the cladding during an accident, the fuel could come into contact with the coolant. If this latter is water, as in most reactors, strongly oxidizing conditions can be produced, under which the oxygen content of the fuel can be significantly increased. Hence, a precise knowledge of the fuel melting-point dependence on the oxygen content is also of primary importance for the analysis of hypothetical mishaps. On the other hand, the experimental determination of the melting behavior of the species UO_{2+x} and U_3O_8 constitutes a big challenge, due to the poor stability of these compounds at high temperature and to their high volatility.

In this work results are presented as obtained by use of a new experimental method recently developed at the Institute for Transuranium Elements (ITU) – Karlsruhe. This method, based on laser heating of the sample surface kept under high buffer gas pressure, permitted the experimental determination of the melting line of stoichiometric UO_2 and of the solidus and liquidus lines of the hyperstoichiometric oxide UO_{2+x} [2–5]. Also, an indicative melting point of the oxide U_3O_8 under a buffer gas pressure of 100 MPa has been obtained, which is presented in this work for the first time.

2. EXPERIMENTAL

The basic principles of the method used here attempted to overcome difficulties that in the past hindered the only existing measurements on the melting behavior of uranium oxides with $O/U \geqslant 2$. These measurements were performed by Latta and Fryxell [6], who used a conventional technique. Their difficulties were mainly linked to the high non-congruent evaporation rate and to the contamination of uranium dioxide with the containing crucible material [7].

In the current research, a pulsed laser beam was used to heat part of the sample surface above the melting point, thus creating "containerless" conditions and avoiding the contact of the molten zone with any external contaminant. Moreover, the sample was kept under a pressurized buffer gas atmosphere (up to 300 MPa) aimed at suppressing as much as possible the evaporation from the heated surface. Classical diffusion of the vapor into the buffer gas was practically ruled out by setting sufficiently high buffer gas pressure and sufficiently short experiment duration. However, within the boundary layer in the vicinity of the sample surface [8, 9] more significant mass transport could take place by laminar convection. Only for a suitable buffer gas pressure and geometrical setup, obtained by setting a protective window 1 mm above the sample surface, could these phenomena be controlled and their effects be kept under the required limits. Among the inert gases, helium was chosen as the buffer gas because it possesses the best optical properties.

Temperature measurements were performed by means of a high-speed pyrometer focused on the sample surface in the center of the laser focal spot. Solidus and liquidus points were determined both visually and by observing the corresponding thermal arrest on the recorded thermograms. A mathematical model was developed to simulate the experiments in order to obtain a better interpretation of the thermograms [4].

A further method of investigation was also developed in order to overcome uncertainties mainly linked to the complex melting process in the presence of temperature and concentration gradients within the sample. A probe laser beam was directed onto and reflected by the sample surface. Analysis of variations in the reflected light signal (RLS) intensity during an experiment permitted the detection of the exact moments at which melting and freezing occurred. Thus, the occurrence of a phase transition on the surface could be detected independently of the complex phenomena that accompanied the propagation of the melting–freezing front in the bulk.

The experimental apparatus used here is presented in Fig. 1. The sample was held vertically inside a high-pressure cell. Its lateral surface was wrapped in a Teflon ring preventing the specimen from breaking under the thermal stresses. Pressures of the order of 0.1 GPa proved to be sufficient to prevent evaporation from the specimen surface. Convective motions in the buffer gas were avoided by placing a thin sapphire protective window 1 mm above the sample surface. The beams produced by two separate Nd:YAG pulsed-laser cavities (total power of ≈ 3 kW for several tens of ms) were merged and channeled in the same optical fiber and, hence, simultaneously focused onto the sample surface. The first laser head supplied the "power pulse," heating the sample above the melting point; the

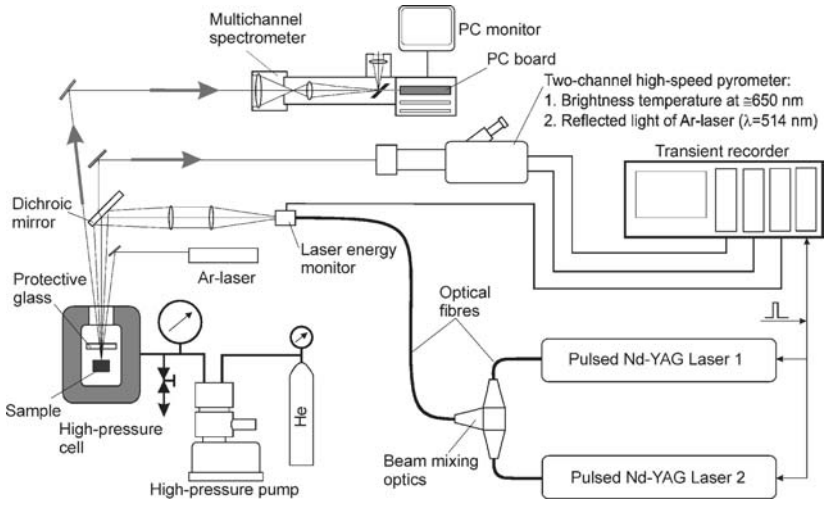

Fig. 1. Experimental setup used in this research.

second one, separately controlled in intensity and duration, delivered a longer pulse of lower power, ensuring conditioning of the sample cooling rate. Thus, the sample temperature was prevented from decreasing too rapidly, and undesirable undercooling of the liquid below the freezing temperature was avoided. The random mixing of the laser radiation inside the optical fiber resulted in a single combined laser pulse with a complex power-time profile at the exit of the focusing optics (recorded by an energy detector), and in a homogeneous power density distribution over the focal spot of 3 mm diameter on the sample surface. Pulses were never repeated on the same specimen, because the surface of a specimen was generally spoiled after a measurement.

The temperature of the sample surface was measured by a high-speed (total time resolution of 10 μs), two-channel pyrometer [10, 11]. The signals of the pyrometer and of the energy detector were transferred to a Nicolet Pro 44C transient digitizer and to a PC.

The first pyrometer channel, operating at 644 nm (half-bandwidth = 15 nm) and calibrated against a standard gas band-lamp, was used for temperature measurements with an uncertainty better than 0.5% at 2500 K. The obtained brightness temperature was converted into true temperature by correcting it for the sample emissivity, taken from Ref. 12, and for the total transmittance of the optical path. This latter was directly determined by means of a probe laser. Both sample emissivity and optical

transmittance of the system were also measured *in situ* with an additional 256-channel pyrometer focused on the sample surface.

The reflected light signal (RLS) analysis introduced above was realized by means of an Ar probe laser ($\lambda = 514$ nm) focused on the sample surface in the center of the zone concerned with the melting–freezing process. The fraction of the 514-nm light reflected by the surface and detected by the second channel of the pyrometer (tuned at the same wavelength) depended on the angular reflectivity of the sample. During the heating stage of an experiment, the first appearance of liquid on the surface caused a sudden change in the angular reflectivity leading to a well defined variation in the light signal. Vibrations of the liquid mass resulted in oscillations of the reflected light intensity, and both disappeared when the freezing point was reached on the cooling phase. In this way, the moments and, by comparison with the 644-nm channel thermogram, the temperatures of first appearance of the liquid phase on the solid surface (solidus) and of formation of the first solid seed in the liquid pool (liquidus) were easily and straightforwardly detectable. This method has also been called the "oscillating directional reflectivity" (ODR) technique.

A typical melting-point measurement performed on a $UO_{2.17}$ sample is presented in Fig. 2. In the first part of the experiment, under high-power laser irradiation, equilibrium conditions were created only on an extremely thin layer on the sample surface, so that the thermogram showed no thermal arrest upon melting. Moreover, since the thermal conductivity is approximately the same both in solid and liquid uranium dioxide [12], heat transport dynamics were practically unaltered during the heating stage both before and after the formation of liquid inside the sample. For this reason, not even an inflection could be observed at the melting temperature in the ascending flank of the thermogram. On the cooling stage, instead, when the liquid mass was allowed to cool naturally and equilibrium conditions were attained, upon freezing, in the whole solidifying mass, a clear inflection could be observed corresponding to the liquidus transition. A further significant recalescence leading to a thermal arrest systematically occurred at a lower temperature in highly hyperstoichiometric samples only. The origin of this phenomenon is still uncertain, as it cannot correspond to any purely thermodynamic phase transition. Since it occurred in oxygen-rich, non-congruently melting samples only, it could be possibly related to displacement of the last oxygen-enriched liquid mass at the end of the freezing process or to redistribution of the oxygen during the final stage of the solidification.

The experiment was simulated with a one-dimensional code described in Ref. 4. The simulated thermogram is in good agreement with the experimental one only up to the liquidus point on the cooling flank of the curve.

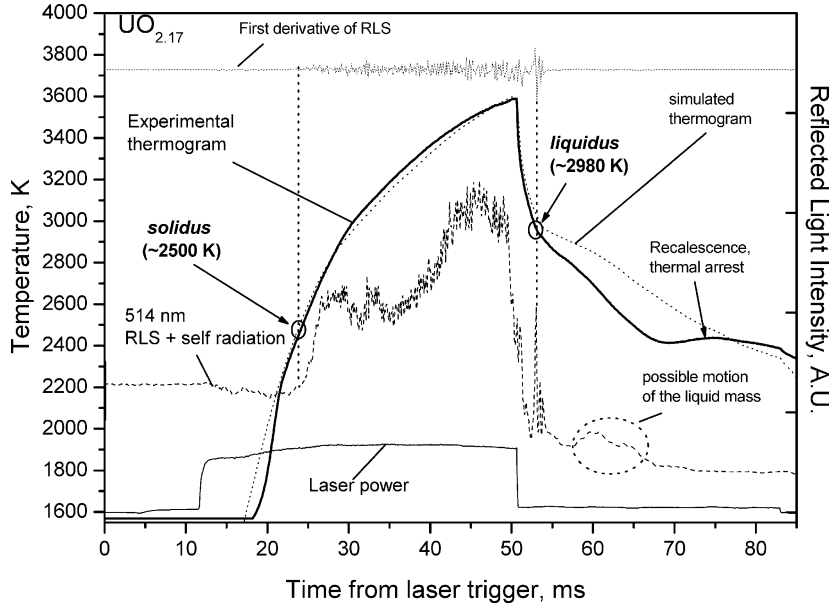

Fig. 2. Example liquidus–solidus measurement on a UO2.17 sample. The solidus was identified by observing the onset of vibrations – due to the formation of liquid on the sample surface – in the reflected light signal (RLS) and in its derivative. The liquidus was detected by means of the clear inflection on the cooling flank of the thermogram, which corresponded to the formation of the first solid seed in the liquid pool, revealed by a peak in the RLS. After this point, vibrations in the RLS continued for another few milliseconds until the complete disappearance of the liquid from the solid surface.

This would confirm after this point that radial diffusion or movement of the liquid could take place in the final stage of the solidification process. Independently of all these effects, the solidus and liquidus temperatures could be determined by means of the reflected light analysis. Vibrations appear and disappear on the reflected light signal curve and, even more clearly, on its derivative, corresponding to the onset of fusion (solidus) during the heating, and to the onset of solidification (liquidus) during the cooling.

3. SAMPLES

Nuclear grade urania pellets, fabricated by Advanced Nuclear Materials Co., were annealed in a flux of Ar + 5% H_2 at 1273 K to ensure that their composition was stoichiometric. The sintered density was better than 95% of the theoretical value ($10.95\,g \cdot cm^{-3}$). The sample composition was

determined by thermogravimetric measurements from the change in the sample mass at full oxidation to U_3O_8 in air. The O/U atomic ratio after annealing was 2.00 ± 0.005. Hyperstoichiometric samples were prepared by treating stoichiometric pellets in an Al_2O_3 furnace at different temperatures under a CO/CO_2 flowing mixture of suitable composition, according to the $UO_{2\pm x}$ Ellingham diagram [13]. Again, the final composition was measured by the difference between the sample masses before and after the treatment, and then confirmed by thermogravimetry within an uncertainty of ± 0.01 on the O/U ratio.

U_3O_8 samples were prepared by sintering "green pellets" (obtained by cold pressing of U_3O_8 powders) for 6 h at 1450 K in a 0.1 MPa oxygen flux. No significant phase composition change was observed following the sintering treatment, as verified by x-ray diffraction (XRD) measurements. The homogeneity of the samples was confirmed through optical and scanning electron microscope (SEM) ceramography.

4. RESULTS

The melting point of stoichiometric $UO_{2.00}$ was already measured, through the method presented here, at several buffer gas pressures as presented in Ref. 3. The good agreement between the measured melting slope dT_m/dP ($92.9\,K \cdot GPa^{-1}$) and the one calculated by substituting existing thermodynamic data in the Clausius–Clapeyron equation ($93.3\,K \cdot GPa^{-1}$) confirmed that conditions of local thermodynamic equilibrium were effectively attained in the molten pool formed on the sample surface. Thus, the method could be reliably applied to more complex systems, such as UO_{2+x} and U_3O_8. Preliminary results on the liquidus and solidus lines of the system were already published [3, 4]. Now further investigation on a larger number of samples and under different experimental conditions (buffer gas pressure, time regime) has confirmed the solidus and liquidus temperatures measured for the hyperstoichiometric compound UO_{2+x} in the composition range $2 \leqslant x \leqslant 2.21$. In particular, experiments with different durations of the heating laser pulse were realized, in order to confirm that the measured phase-transition temperatures were independent of uncontrollable effects taking place during the melting–freezing process. These effects mainly consisted of segregation in the solid, displacement of the liquid mass during the freezing process, and of expansion of the boundary layer in the surrounding gas, hence, of convective diffusion of the vapor from the sample surface.

Figure 3 shows a comparison between two melting-point measurements performed on a $UO_{2.16}$ sample with laser pulses of different duration. In experiment A, the sample surface was kept over the melting (solidus) point

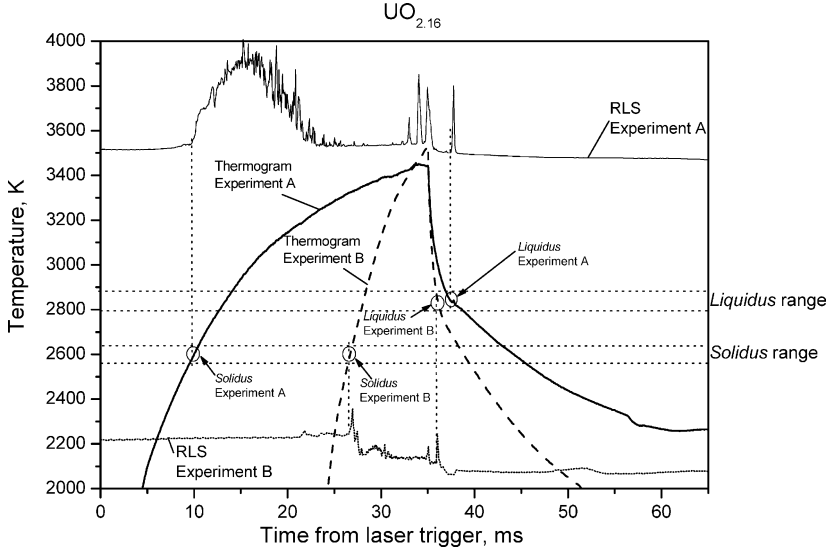

Fig. 3. Comparison between two melting-point measurements performed on a $UO_{2.16}$ sample with different time regimes. In experiment A, the sample surface was kept over the melting-point (solidus) for several tens of milliseconds, whereas in experiment B the existence of the liquid phase was limited to about 12 ms. Solidus and liquidus points measured by means of reflected light signal (RLS) analysis agreed in the two cases, within the uncertainty limits indicated by solid circles.

for several tens of milliseconds, whereas in experiment B the existence of the liquid phase was limited to about 12 ms. Solidus and liquidus points measured by means of reflected light signal (RLS) analysis agreed in the two cases, within the uncertainty limits indicated by solid circles. Such a result would not have been obtained if the error induced by the hypothetical time-dependent segregation, liquid displacement, and vapor convection phenomena had been decisive. It is interesting to remark that no recalescence was observed at the end of the freezing stage in the shorter experiment. This was well reproducible in short-duration melting point experiments, and could be related to the fact that in this case displacement of the liquid enriched in oxygen could not have the time to occur.

Similar melting experiments were performed on U_3O_8 specimens. In this case, only maximum temperatures of a few tens of kelvins above the melting point could be reached, because higher temperatures would have led to strong evaporation from the sample surface. In this way, however, only a small volume of material was melted, and practically no plateau could be observed on the cooling flank of the thermogram at the freezing

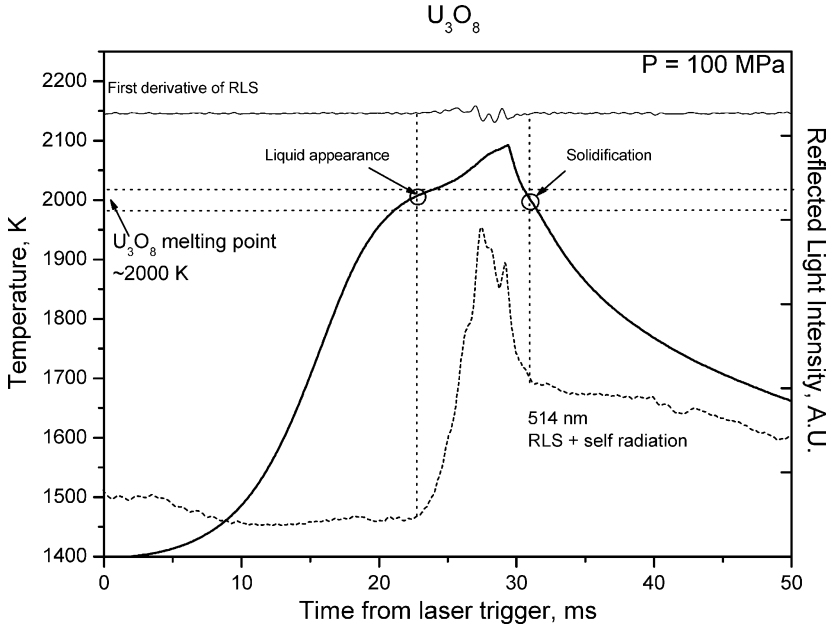

Fig. 4. Melting-point measurement performed on a U_3O_8 sample. The sudden variation of superficial reflectivity in the reflected light signal (RLS) corresponds to the presence of liquid on the sample surface. Clear traces of solidified liquid on the surface of the specimen were observed with the optical microscope after the melting–freezing experiment. Slight inflections on the thermogram (black thick line) recorded by the 644 nm channel are visible at the melting and freezing points.

point. A typical melting-point measurement of this kind, with a buffer gas pressure of 100 MPa, is shown in Fig. 4. Under these conditions the RLS analysis would indicate a melting point of about 2010 K. In this case a thermal arrest is observable in the same temperature range, probably due to a significant difference between the thermal conductivity of the solid and that of the liquid in U_3O_8, and also to the increase, after melting, of the evaporation rate. The same temperature range for the melting point of U_3O_8 was obtained by performing a "visual test" in which the specimen was heated in successive shots at increasingly higher maximum temperatures. After each shot the specimen surface was observed with the optical microscope, and possible formation of liquid was checked from topographic changes. The melting temperature should be situated above the maximum temperature reached in the last shot in which no liquid was formed, and below the maximum temperature of the first shot where signs of fusion were detectable on the sample surface. The same sort of test on UO_{2+x} samples confirmed the measured solidus points.

Table I. Results Obtained in This Work

Nominal composition (O/U)	Number of samples investigated	Pressure (MPa)	Solidus (K)	ΔT *solidus* (K)	$\Delta(O/U)$ *solidus*	Liquidus (K)	ΔT *liquidus* (K)	$\Delta(O/U)$ *liquidus*
2	19	100	3147	±20	±0.005	3147	±20	±0.005
2.01	6	100	3071	±20	±0.005	3135	±20	±0.005
2.03	6	100	3055	±25	±0.005	3130	±20	±0.005
2.03	3	150	3060	±25	±0.005	3115	±25	±0.005
2.05	8	100	2964	±50	±0.005	3098	±20	±0.005
2.07	5	50	2948	±40	±0.005	3028	±40	±0.005
2.07	11	100	2958	±40	±0.005	3070	±20	±0.005
2.07	4	200	2954	±40	±0.005	3063	±40	±0.005
2.08	12	100	2886	±25	±0.01	3075	±20	±0.01
2.09	9	100	2901	±49	±0.005	3056	±25	±0.005
2.11	8	100	2793	±40	±0.005	2995	±20	$-0.005 + 0.015$[a]
2.12	9	100	2699	±25	±0.01	3008	±20	$-0.01 + 0.02$[a]
2.12	3	120	2696	±25	±0.01	3020	±25	$-0.01 + 0.02$[a]
2.14	7	100	2607	±25	±0.01	2930	±40	$-0.01 + 0.03$[a]
2.16	5	10	2606	±30	±0.01	2920	±30	$-0.01 + 0.035$[a]
2.17	3	50	2528	±50	±0.005	2887	±50	$-0.005 + 0.04$[a]
2.17	5	100	2550	±50	±0.005	2891	±25	$-0.005 + 0.04$[a]
2.17	3	200	2530	±50	±0.005	[b]	[b]	[b]
2.2	12	100	2438	±35	±0.005	2865	±30	$-0.005 + 0.055$[a]
2.21	10	100	2410	±25	±0.005	2795	±60	$-0.005 + 0.059$[a]
2.66 (U_3O_8)	10	100	2010	±75	±0.005[c]	2010[d]	±100[d]	[c]

[a] Uncertainty in the sample composition including the possible oxygen segregation upon freezing.
[b] Unsuccessful measurement.
[c] Starting composition: stoichiometric U_3O_8 within the experimental uncertainty. Final composition not measured.
[d] Uncertain freezing temperature estimated on the basis of RLS analysis.

The provisional results presented here on the fusion temperature of U_3O_8 can be regarded as the first experimental information in a domain of the U–O phase diagram where data are still lacking. However, due to the high volatility of U_3O_8, further measurements will be required in order to better establish the minimum buffer gas pressure at which evaporation can be actually neglected.

The experimental data measured in this research are shown in Table I with the statistical uncertainty (standard deviation) of each value. The uncertainty range associated to the liquidus composition of the most oxidized samples is asymmetrically extended towards higher oxygen contents to consider, in a conservative fashion, the possible effect of segregation on the actual composition of the liquid upon freezing. The extent of this effect was estimated on the basis of computer simulation results [4, 5].

5. DISCUSSION

Figure 5 reports the solidus and liquidus lines measured in this work for UO_{2+x} in the range $0 \leqslant x \leqslant 0.21$. The external pressure dependence of the points measured proved to be negligible compared to the precision of the measurements themselves. The horizontal error bands associated with each experimental point represent the uncertainty in the exact composition of a single specimen, determined by thermogravimetry. In the most oxidized samples, horizontal error bands for the liquidus point are asymmetrically extended towards higher oxygen contents according to the uncertainty reported in Table I (dotted arrows in the figure). Vertical uncertainty bands indicate the standard deviation in the reproducibility of each experimental value. All numerical values are reported in Table I.

The points obtained are compared with those measured by Latta and Fryxell [6] in 1970 with a conventional thermal arrest method. The results of Latta and Fryxell were affected by the extensive contamination of the samples with the crucible metal (W or Rh) [7]. Moreover, in the hyperstoichiometric UO_{2+x} samples investigated in Ref. 6, important losses of the excess oxygen occurred, as the oxygen would easily diffuse into the metal crucible during the melting–freezing process that normally lasted several hours. The actual oxygen content of these samples at the melting point was therefore most probably lower than that measured by Latta and Fryxell before their experiments. This would shift their solidus and liquidus lines towards lower oxygen contents, explaining the fact that the temperatures proposed by them are systematically higher than those presented here.

Our liquidus and solidus lines are in fair agreement with those calculated by Babelot et al. [14], also shown in Fig. 5. The U–O system

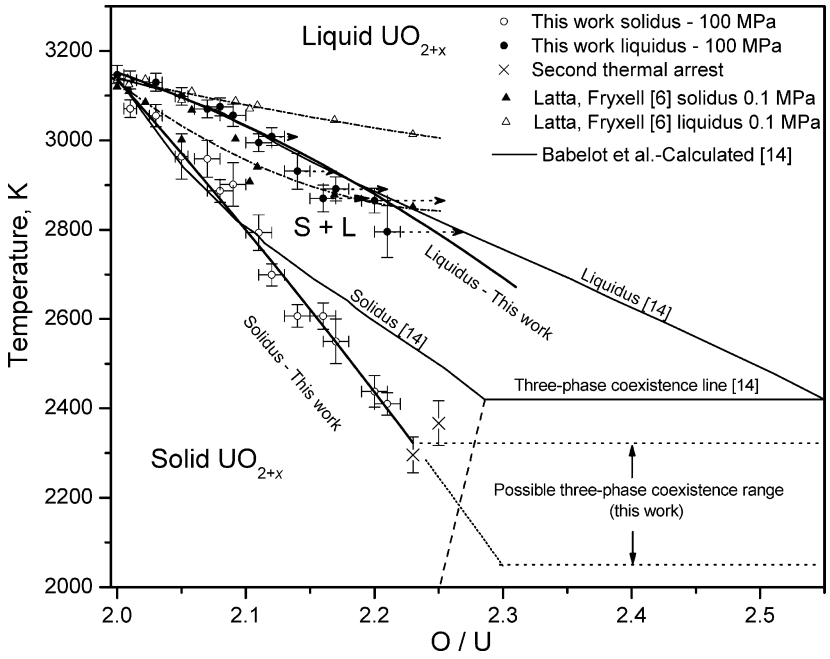

Fig. 5. Phase diagram of the U–O system in the vicinity of the melting transition in the range $2 \leqslant O/U \leqslant 2.55$. The points measured in this work are compared with those measured by Latta and Fryxell [6], and with the phase diagram calculated by Babelot et al. [14]. In the most oxidized samples, horizontal error bands for the liquidus points are asymmetrically extended towards higher oxygen contents (dotted arrows) to take into account the possible effect of segregation on the actual composition of the liquid upon freezing.

was represented in Ref. 14 as a mixture of the three species U, UO_2, and UO_3. The interaction model of Hoch and Arpshofen [15] was used to calculate the free energy of the solid mixture UO_{2+x} and of the liquid, while the Schottky–Wagner disorder model [16] was used in calculations for compositions close to stoichiometric UO_2. The monotectic line calculated in Ref. 14 represents the coexistence of the phases UO_{2+x} (s)/UO_{2+x} (l)/U_3O_8 (l). A similar three-phase coexistence line is foreseen in several other calculations of the U–O phase diagram (see, for instance, Refs. 17 and 18). These latter calculations were calibrated on Latta and Fryxell's data, and yielded therefore results, not shown in Fig. 5, in poorer agreement with the experimental values obtained in the current research. The "thermal arrest" occurring at the end of the cooling stage in thermograms recorded for hyperstoichiometric samples (see Section 3) would

correspond, in the specimens with the highest oxidation level, to the lowest temperatures at which liquid UO_{2+x} was ever observed, constituting an upper bound for the mentioned three-phase transformation line. These temperatures are indicated by two "×'s" around 2300 K in Fig. 5. On the other hand, our estimate of the melting temperature for the U_3O_8 oxide (Section 4) would suggest that such a line could be expected at a temperature closer to approximately 2000 K. All these considerations are valid only if the formation of gas is neglected, which is certainly a reasonable assumption under the conditions realized in our experiments.

6. CONCLUSIONS

A new experimental method for the investigation of phase transitions in high-melting and volatile materials, already presented in previous publications, was used in this work for a more extended study of the behavior of hyperstoichiometric uranium dioxide and for a first estimate of the melting point of the U_3O_8 oxide. Obtained results can constitute the basis for a better assessment of the U–O phase diagram in the oxygen-rich region.

ACKNOWLEDGMENTS

The authors wish to thank J. Spino and J. Somers for their help in the preparation of the samples, C. Ronchi for his valuable suggestions, and W. Heinz and U. Zweigner for their technical support.

REFERENCES

1. N. N. Greenwood and A. Earnshaw, *Chemistry of the Elements* (Pergamon Press, Oxford, 1984).
2. D. Manara, C. Ronchi, and M. Sheindlin, *Int. J. Thermophys.* **23**:1147 (2002).
3. D. Manara, C. Ronchi, and M. Sheindlin, *High Temp.-High Press.* **35–36**:25 (2003–2004).
4. D. Manara, M. Sheindlin, and M. Lewis, *Int. J. Thermophys.* **25**:533 (2004).
5. D. Manara, *Melting Transition Measurements in Uranium Dioxide*, Ph.D. Thesis (Department of Physics, University of Warwick, 2004).
6. R. E. Latta and R. E. Fryxell, *J. Nucl. Mater.* **35**:195 (1970).
7. M. H. Rand, R. J. Ackermann, F. Groenvold, F. L. Oetting, and A. Pattoret, *Rev. Int. Hautes Tempér. Réfract. Fr.* **15**:355 (1978).
8. J.-P. Hiernaut and C. Ronchi, *High Temp. – High Press.* **21**:119 (1989).
9. E. R. G. Eckert, *Heat and Mass Transfer* (McGraw-Hill, New York, 1959).
10. M. Sheindlin, *Sov. Tech. Rev. B. Therm. Phys.* **4**:1 (1992).
11. M. Sheindlin and V. N. Senchenko, in *Proc. of the International Symposium on Major Problems of Present-Day Radiation Pyrometry* Moscow (1986), p. 220.
12. J. K. Fink, *J. Nucl. Mater.* **279**:1 (2000).

13. T. B. Lindemer and T. M. Besman, *J. Nucl. Mater.* **130**:473 (1985).
14. J.-F. Babelot, R. W. Ohse, and M. Hoch, *J. Nucl. Mater.* **137**:144 (1986).
15. M. Hoch and I. Arpshofen, *Z. Metallk.* **75**:23 (1984).
16. C. Wagner and W. Schottky, *Z. Phys. Chemie* **B11**:163 (1931).
17. C. Guéneau, M. Baichi, D. Labroche, C. Chatillon, and B. Sundman, *J. Nucl. Mater.* **304**:161 (2002).
18. P.-Y. Chevalier, E. Fischer, and B. Cheynet, *J. Nucl. Mater.* **303**:1 (2002).